JOURNAL OF SOLID STATE CHEMISTRY 91, 189–203 (1991)

HREM of Electron-Beam-Induced Damage in L-Ta_2O_5

T. R. WAGNER[1]

Center for Surface Radiation Damage Studies, Department of Materials Science & Engineering, Northwestern University, Evanston, Illinois 60208

Received January 19, 1990; in revised form June 25, 1990

Samples of L-Ta_2O_5 exposed to a high current density electron beam were observed by high resolution electron microscopy (HREM) to reduce to suboxide and metallic Ta phases. Data are presented for crystals aligned along [001], [020], [200], and [130], in which surface areas are seen to reduce to Ta_2O, TaO_2, bcc Ta, or a β-Ta phase via an amorphous intermediate phase. The driving force appears to involve desorption of oxygen stimulated by electronic transitions (DIET), and the possible involvement of the "infinitely adaptive nature" of the initial L-Ta_2O_5 structure in the damage process is discussed. Comparison of results obtained from an ultrahigh vacuum HREM to those from a conventional HREM suggests that contamination effects in lower vacuum systems influences the reliability of the results, especially in complex systems like Ta-O. Finally, the results follow a symmetry selection rule, which explains why L-Ta_2O_5 does not reduce to the monoxide phase as observed in similar experiments with TiO_2, V_2O_5, and Nb_2O_5.

Introduction

High resolution electron microscopy (HREM) studies of electron-beam-induced damage in oxides has been an area of increasing interest during recent years. Much of this work has concentrated on maximally valent transition metal oxides, in which damage involves the loss of oxygen from the specimen surface accompanied by a reduction of the metal atom to a lower oxidation state. The basis for this argument comes from conventional surface science studies in which oxygen loss from the surface is detected directly (*1*), as well as from empirical observations made from the electron micrographs and diffraction patterns. A well-known mechanism used to explain this type of oxygen loss (which occurs in the microscope at energies below the threshold for knock-on damage) is referred to as desorption induced by electronic transitions (DIET) (*2*, *3*). DIET processes occurring in the electron microscope have been reported as being the main driving force leading to damage in compounds such as WO_3 (*4–6*), MoO_3 (*7*), TiO_2 (*5*, *8*), V_2O_5 (*5*, *9*), and Nb_2O_5 (*5*).

Of equal importance to understanding the primary driving force initiating damage processes in such studies, of course, is understanding the structural relationships among the initial, intermediate, and final phases which exist during the damage process. Obviously it is in this latter area where the electron microscope is particularly well-suited to contribute information. In this paper observations of beam-induced damage in L-Ta_2O_5 (i.e., low temperature form) uti-

[1] Current address: Dept. of Chemistry, Illinois Institute of Technology, Chicago, IL 60616.

0022-4596/91 $3.00

lizing both conventional and ultrahigh vacuum (UHV) HREMs are presented, and the crystal chemistry involved in the damage process in described. To my knowledge, no data involving the beam-induced damage of this material in a HREM have yet been reported. The observations are consistent with the DIET mechanism. Before discussing the damage results, the structural properties of the initial L-Ta_2O_5 sample will be described, as these are somewhat complex and may be involved in the damage mechanism.

Experimental

The L-Ta_2O_5 sample consisted of powder obtained from Johnson Matthey Chemicals Ltd. Most of the results presented herein were obtained from an Hitachi H-9000 HREM operated at 300 and 100 keV under a vacuum of 10^{-7} Torr. Other results were obtained from a dedicated UHV H-9000 HREM at 300 keV with the instrument operating at a working vacuum (at the specimen region) of 2×10^{-10} Torr. Samples for HREM were prepared by crushing the powder in an alumina morter and pestle, and scooping fine particles from an acetone suspension onto a copper grid typically coated with a holey carbon film. SiO support films were used instead of holey carbon for the UHV specimens. Before being introduced into the UHV microscope column, the sample was heated to temperatures up to 150°C for 8 hr during bake-out of the specimen transfer chamber. Specimens for the conventional H-9000 were baked on a light bulb for 10 min before insertion into the microscope column to reduce effects due to air contaminants.

The Northwestern University multislice image simulation (NUMIS) programs were utilized to obtain calculated images and diffraction patterns of the starting material. Regions of images showing surface phase contrast too small (<1000 Å^2) to analyze by SAED were analyzed using optical diffractograms obtained from a standard laser optical bench.

Initial Structure

Most of the early papers (*10–12*) on the structure of L-Ta_2O_5 agreed that the strong reflections in the respective X-ray data could be indexed as an orthorhombic unit cell with parameters a = 6.2 Å, b = 3.66 Å, and c = 3.898 Å, corresponding to the α-UO_3-type structure. However, much confusion arose due to discrepancies in the positions of weak lines appearing on powder patterns obtained by the various workers, which suggested that different specimens consisted of structures with different superlattice multiplicities. Structural studies on L-Ta_2O_5 and compounds in the Ta_2O_5–WO_3 system by Roth and Stephenson (*13*) removed the confusion by demonstrating how subcell units can stack in various ways to form structures of different multiplicities, as depicted in Fig. 1.

The basic building blocks of the structure consist of subcell units having the ideal U_3O_8 structure, as shown in Fig. 1a. In Fig. 1b, a folding plane is introduced following the stacking of each U_3O_8-type cell. At the folding planes, pairs of octahedra are corner-shared and the (110) plane becomes a mirror plane. The figure indicates that there are actually two types of folding planes relative to the U_3O_8-type subcells. One type (i.e., at the left and right arrows) is basically a (110) twin, while the other (middle arrow) involves interpenetration of the (110) planes, resulting in a composition slightly deviated from M_3O_8. The stacking of subcells in this way results in the formation a new unit cell, which can be described as 5 UO_3-type cells stacked along their b-axes as shown. If n is the number of U_3O_8-type unit cells stacked before a folding plane is introduced, then the multiplicity (i.e., the number of UO_3-types along the b-axis) of the resulting unit

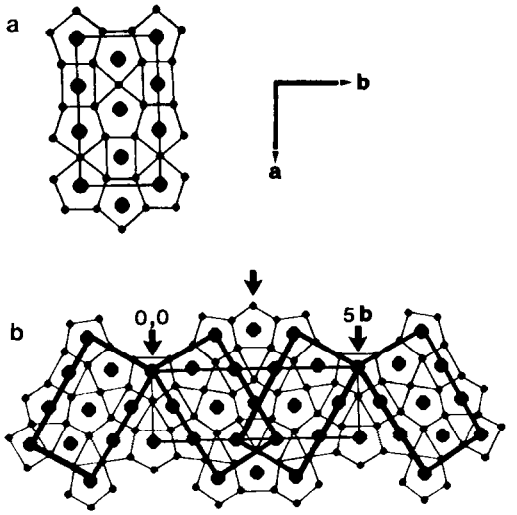

FIG. 1. Structure-building principle for L-Ta_2O_5 structures. Large spots represent metal atoms and small ones oxygen atoms: (a) U_3O_8-type basic building block in [001] projection, $z = 0$. The three-dimensional structure consists of a mirror at $z = 0.5$, where bridging oxygen atoms above and below each metal atom are also located. (b) Formation of structure containing five UO_3-type cells, resulting from the introduction of a folding plane following the stacking of each U_3O_8-type cell. The ideal composition is $M_{10}O_{26}$. Thick lines outline the U_3O_8-type cells; positions of folding planes are arrowed.

cell is $m = 5, 8, 11, 14 \ldots (3n + 2)$. These are the basic structures which can exist in this system, but many other structures are possible by various combinations of these; for example, a structure having $m = 13$ is represented simply as $m = a5 + b8$ (here $a = b = 1$ but they can be any integer in principle).

Because the combination of two or more base structures results in the formation of a third unique structure, biphasic behavior is not observed in this system. The ability of L-Ta_2O_5 to form monophasic fully ordered structures over a certain composition range without creation of point defects led Anderson (*14*) to classify this material as an "infinitely adaptive structure."

The ideal compositions of the structures obtained according to the building principle described above are given as $M_{2m}O_{[16m-2(a+b)]/3}$, and are always oxygen-rich with respect to the composition O/Ta = 2.5. The "real" structure of L-Ta_2O_5 as reported in a structural refinement study by Stephenson and Roth (*15*) has a multiplicity of 11 × *b*. Since the ideal composition of the 11 × *b* is $Ta_{22}O_{58}$, three oxygen atoms are "missing" in order to form the real composition of $Ta_{22}O_{55}$. Stephenson and Roth referred to the oxygen-deficient sites as "distortion planes," and these occur such that the coordination number of some metal atoms is reduced from seven to six. It is important to note that the specimen refined by Stephenson and Roth for this study was annealed for 2 weeks at 1350°C. The initial material reportedly showed powder diffraction reflections corresponding to the 14 × *b* structure, which appears to be the structure of the specimen examined in this study.

As a structural refinement of a 14 × *b* structure has apparently not been reported, the structural building principle discussed above was applied to describe the initial structure of the specimen, and the ideal structure shown in Fig. 2 was obtained. The unit cell of this structure is orthorhombic with $a = 6.2$ Å, $b = 51.28$ Å, and $c = 3.90$ Å. After distortion planes (i.e., removing oxygen atoms) at various sites in the lattice were introduced, attempts were made to simulate the HREM diffraction patterns and images to determine whether the experimental structure corresponded to that expected. It was discovered that a closer match could be obtained by introducing no distortion planes, suggesting that these planes are distributed at random so that the material has an average structure similar to Fig. 2.

In Fig. 3 diffraction patterns calculated using the average structure are compared to experimental ones for the [001] and [200] zones, since these zones reveal the most information regarding the modulated struc-

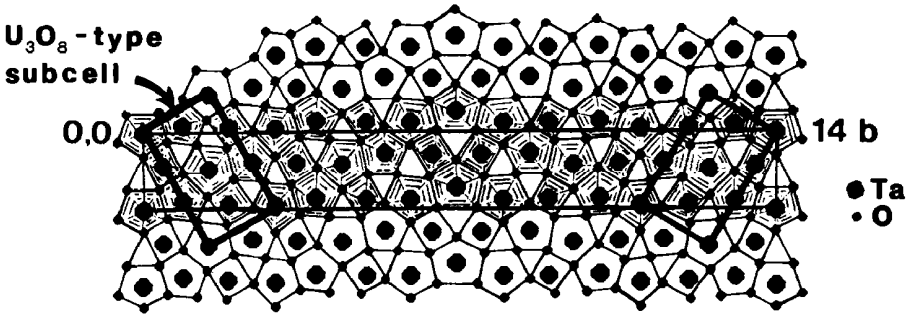

FIG. 2. Ideal structure proposed for the sample used in this study, based on the structure-building principle of Roth and Stephenson (*13*). The structure has a multiplicity of 14 × *b*, where *b* is the *b*-axis of the UO_3-type subcell. U_3O_8-type subcells are outlined by thick lines.

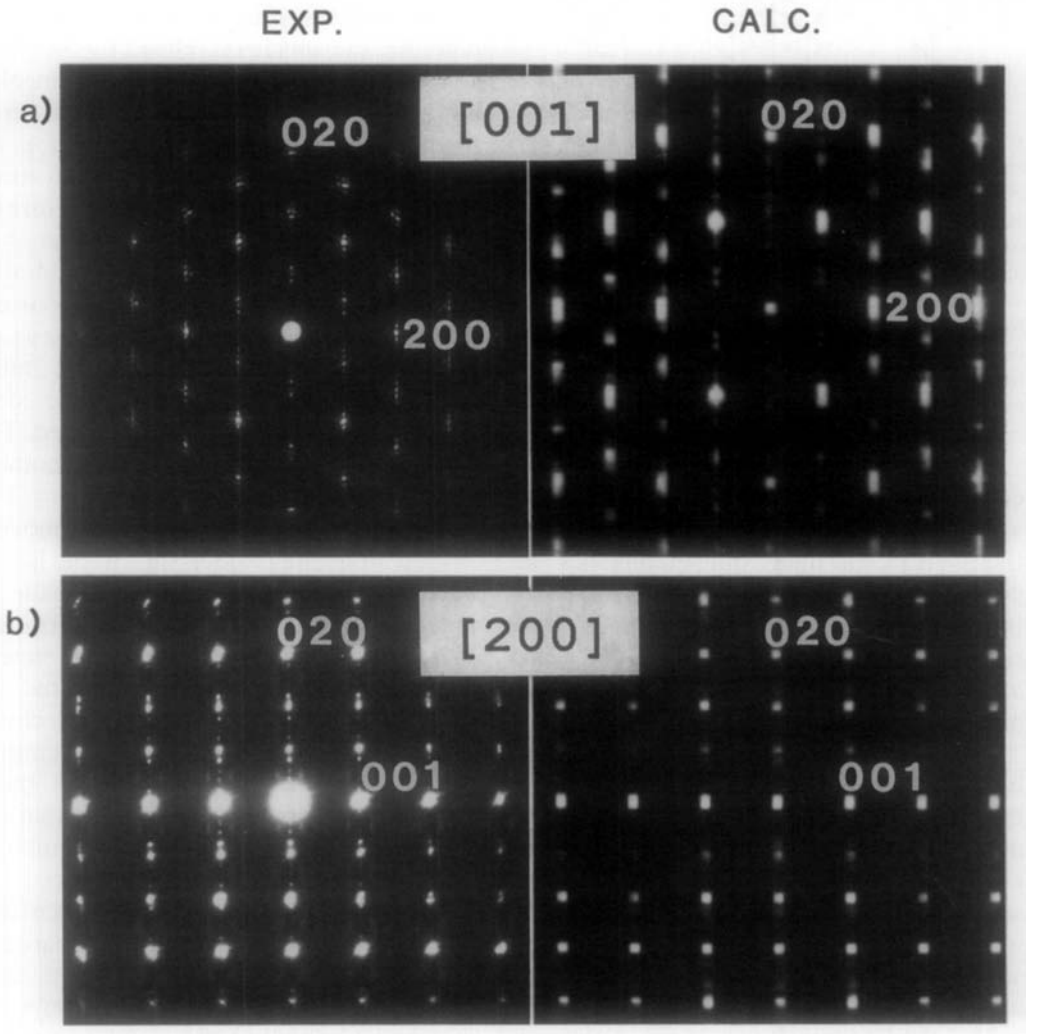

FIG. 3. Experimental and calculated diffraction patterns for the (a) [001] zone. (b) [200] zone.

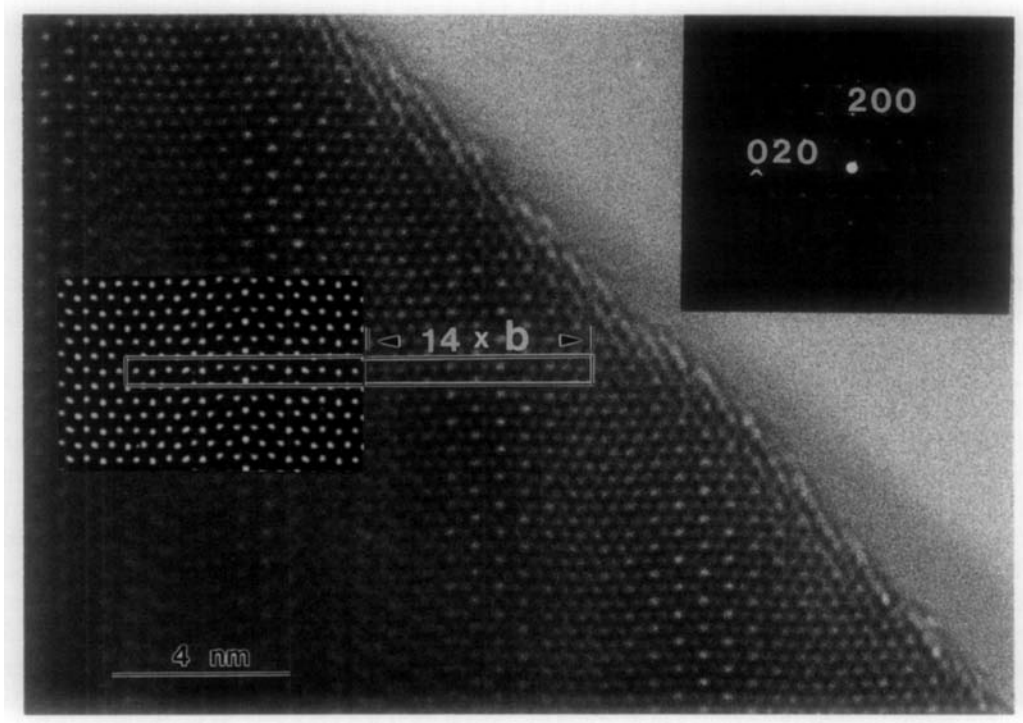

FIG. 4. An [001] image showing columns of Ta atoms in reverse contrast. Inset on the left side is an image calculated from the structure shown in Fig. 2, with defocus = 250 Å and thickness = 31 Å.

ture. The sublattice spots can be indexed according to the ideal α-UO_3-type structure (space group *C2mm*) having the parameters mentioned earlier. The closely spaced spots along (020) in patterns of both zones are due to the 14 × *b* superlattice. The spots at $1/3d_{(020)}$ and $2/3d_{(020)}$ in the [200] patterns are due to the (110) reflections of the U_3O_8-type substructure, as apparent by noting the position of the U_3O_8-type subcell relative to the UO_3-type in Fig. 2. Likewise, the [001] patterns are also indexed by superimposing the patterns of UO_3- and U_3O_8-type substructures.

On the basis of these observations, it would appear that the ideal structure of Fig. 2 does provide a qualitative model for the initial structure of our specimen. However, there is noticeable disagreement between experimental images and images simulated using this model. A typical "best-match" comparison is depicted in Fig. 4. Shown in the left portion of the figure is a simulated image obtained at a defocus of 250 Å and a thickness of 31 Å. The white spots of the simulated image correspond to Ta atoms in reverse contrast and are seen to match the symmetry of the experimental image (which is localized) rather well; however, the relative intensities of specific spots in the respective images do not match. This is apparent by noting that every third spot in the central portion of the outlined region in the image is more intense than the others.

I have attempted to simulate this and other images showing "anomalous" contrast by using structural models slightly modified from that shown in Fig. 2. As mentioned, most of the models which were used involved positioning the distortion planes

at various sites in the lattice. Although the possibility of successfully simulating the images after further trial and error cannot be ruled out, at this point it is concluded that while the Ta atoms appear to be located in the positions expected, there is some anomaly regarding the oxygen positions. It should be pointed out here that the structure also involves weak superlattice ordering along the *c*-axis, and not just in the two-dimensional *a*–*b* plane. This is indicated by diffraction patterns for zones nonparallel to [001], in which satellite reflections are visible around the subcell spots. In the [200] experimental pattern of Fig. 2b, for example, such reflections can be indexed as (0 4 1/6) with respect to the 14 × *b* structure. Therefore it is possible that obtaining successful image simulations would require knowledge of this three-dimensional ordering. No attempts to compute simulations based on 3-D superlattice models have been made, however, since the nature of this structure could be quite complex. For the purposes of this study, qualitative knowledge of the structure as depicted in Fig. 2 is sufficient.

Results

The high stability of the L-Ta_2O_5 structure is evident from the high current-density required to induce damage as compared to other oxides, such as, for instance, Nb_2O_5 and V_2O_5. For most of the specimens examined, damage occurred only after removal of the condenser aperture (fluxes ranged from 150 to 230 A/cm^2) and was limited to surface regions. Irradiation times of up to several hours did not result in complete phase transformation of the bulk material (e.g., as observed in WO_3 (*6*), MoO_3 (*7*), and V_2O_5 (*9*)), and diffraction patterns obtained before and after irradiation differed little, although the final pattern occasionally revealed some evidence of a new phase (see below). Surface phases were therefore most often identified from optical diffractograms.

Specimens in the [001] orientation were observed to damage less readily than those in other orientations, most likely due to the relatively dense layers of Ta atoms normal to the beam. The damage mechanism (i.e., at the surface edge) observed in all orientations involved the transformation to a new structure through an intermediate "amorphous" phase, where this intermediate phase is represented by regions of the image having completely disordered contrast.

This transformation path is illustrated in Fig. 5, which is a time sequence of images from an [001] specimen exposed to a high-flux beam. The image shown in Fig. 5b was obtained after 30 min irradiation time, and comparison with the initial image in Fig. 5a reveals the formation of an amorphous phase at the surface edges. After a total irradiation time of 2.5 hr, the image of Fig. 5c was obtained. Though damage is not extensive, it is apparent that a new phase has formed at the surface edges. The optical diffractogram (OD) taken from the region indicated shows only two planes approximately 90° apart. These planes have similar spacings with values of 2.23 and 2.28 Å, as calibrated from an OD obtained from the bulk region. The closest match to these spacings which could be found after examining several possible phases (see Table I) are the ⟨122⟩ planes of Ta_2O, with $d_{(122)} = 2.23$ Å. Ta_2O reportedly (*16*) has the Cu_2O-type structure with $a = 6.68$ Å. Thus the Ta_2O phase would be aligned along $[66\bar{3}]$, with one of the ⟨122⟩ planes parallel to U_3O_8-type $(5\bar{1}0)$ planes and the other parallel to U_3O_8-type (130) planes. Note that here and throughout all diffraction patterns are indexed for the case of the (020) planes of the U_3O_8-type subcell parallel to the $(\bar{1}10)$ planes of the UO_3-type subcell.

In one instance more extensive damage was observed in an [001] specimen, as seen in Fig. 6. The specimen in this case was rather thick initially, and as might be expected, little damage occurred for some time with the exception of a narrow amorphous

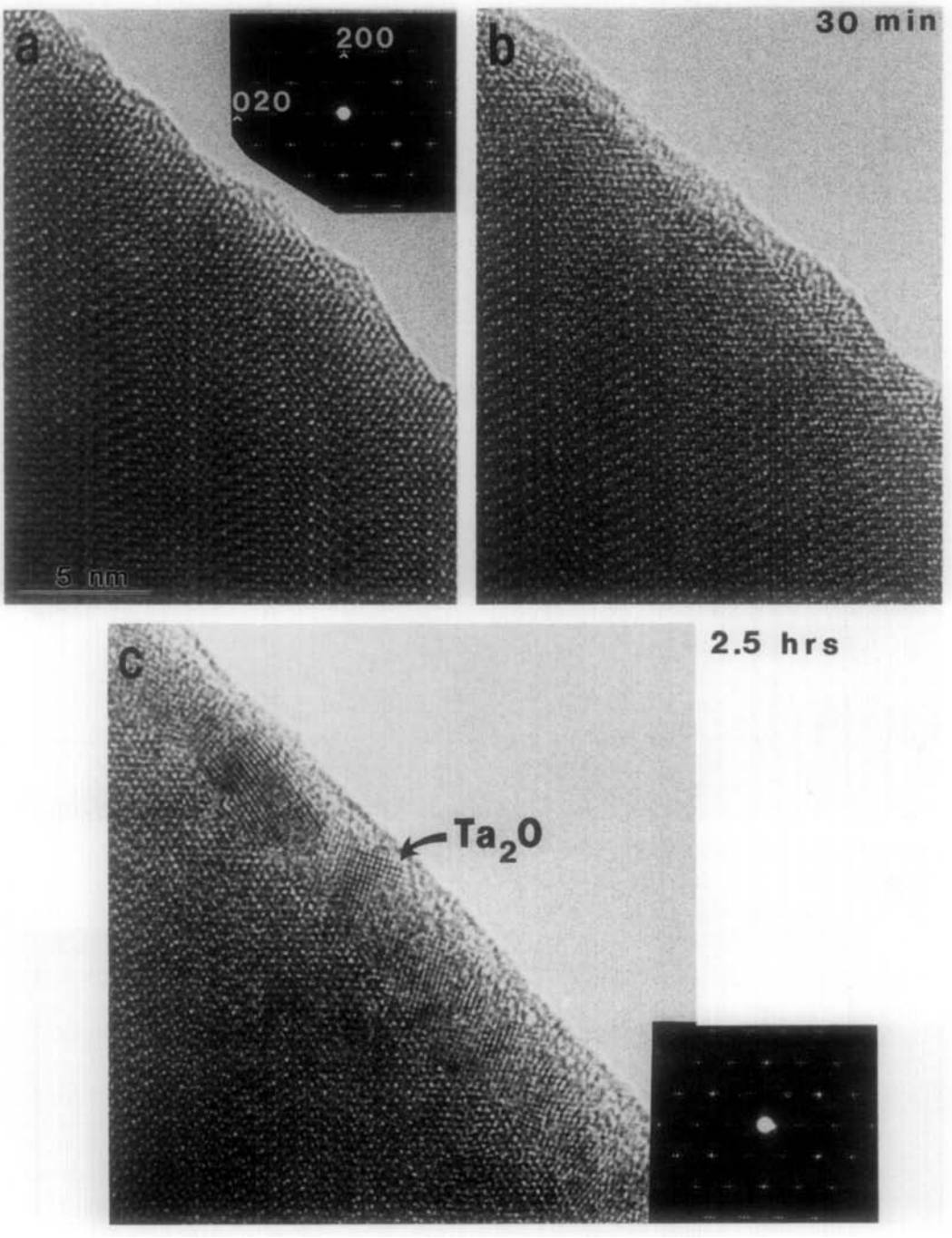

FIG. 5. Time sequence of damage for an [001] crystal: (a) Initial image. (b) Image after specimen exposed to a high-flux beam for 30 min. A thin amorphous layer is visible at the surface edge. (c) Image after 2.5 hr exposure time. Optical diffractogram taken from surface phase at arrowed region was indexed as $[6\bar{6}3]$ Ta_2O.

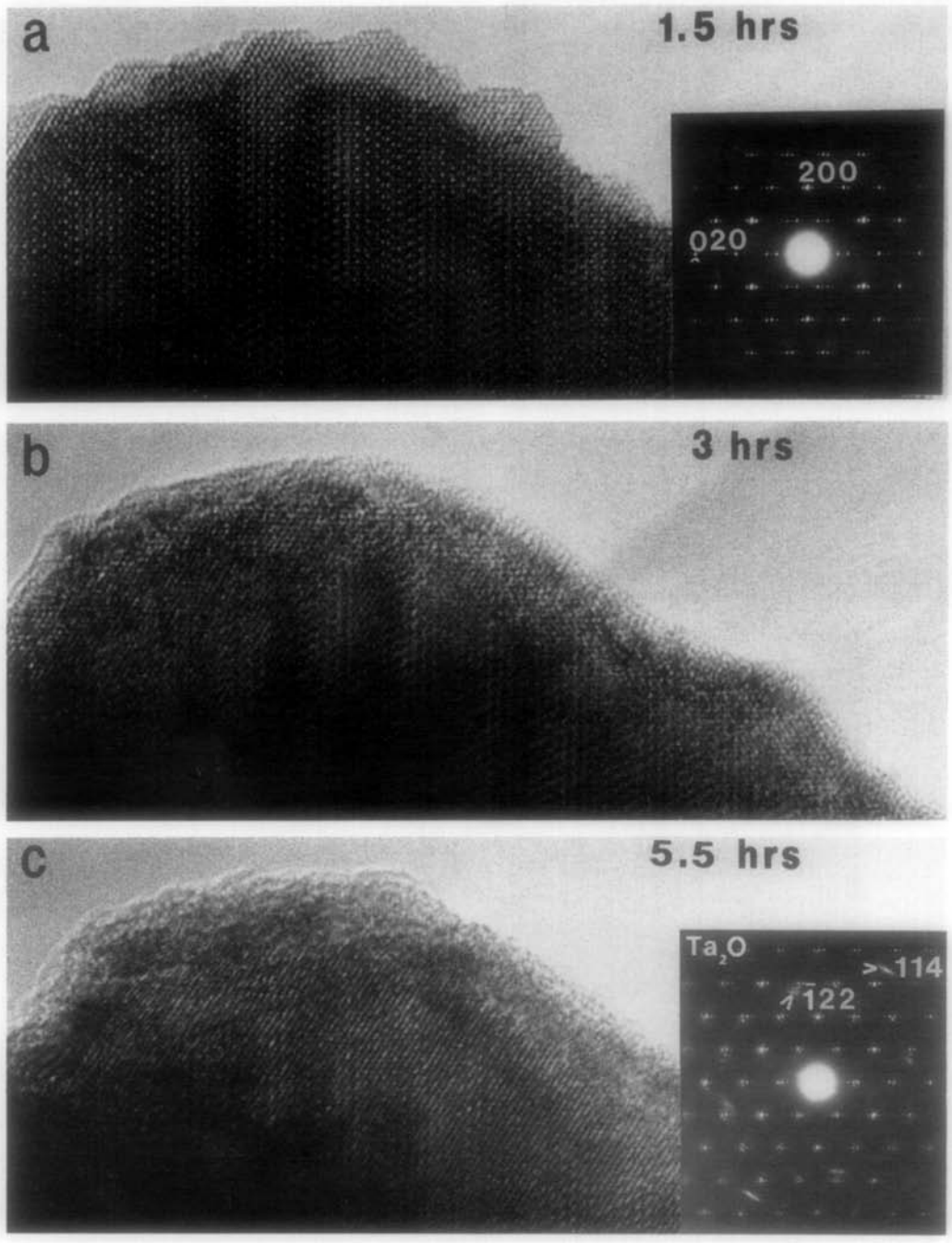

FIG. 6. More extensively damaged [001] crystal: (a) Image after 1.5 hr irradiation time. A portion of the cyrstal broke away, leaving a thin surface edge with undamaged L-Ta_2O_5 structure. (b) After 1.5 hr additional irradiation time, a narrow amorphous layer is visible at the surface edge. (c) After 5.5 hr, a Ta_2O phase is visible on the top surface and at the crystal edges. Spots due to Ta_2O on the electron diffraction pattern are labeled.

TABLE I

Ta–O PHASES USED FOR ANALYSIS OF OPTICAL DIFFRACTOGRAMS OF L-Ta_2O_5 SURFACE PHASES

Phase	Lattice	Parameters (Å)			Space group	Ref.
		a	*b*	*c*		
β-Ta[a]	Tetrahedral	10.19	—	5.31	*P4/mnm*	(17)
β-Ta[a]	Tetrahedral	10.92	—	9.2	Point group *4/mmm*	(18)
β-Ta[a]	Tetrahedral	5.34	—	9.94	Not given	(25)
β-Ta[a]	Hexagonal	2.83	—	5.34	$P6_3/m$	(26)
bcc Ta	Cubic	3.30	—	—	*Im3m*	(25)
$TaO_{1.6}$	Orthogonal	5.47	7.65	26.10	*Pmmm*	(27)
$TaO_{0.95}$	Tetrahedral	3.87	—	3.89	*P4/mmm*	(28)
TaO_2	Tetrahedral	13.32	—	6.12	$I4_1/a$	(29)
TaO_2	Tetrahedral	4.75	—	3.09	$P4_2/mnm$	(30)
Ta_2O	Cubic	6.68	—	—	*Pn3*	(16)
Ta_4O	Orthogonal	7.19	3.27	3.20	*Pmmm*	(31)
H-Ta_2O_5	Monohedral	35.97	3.81	3.81	*C2*	(32)

[a] Literature indicates these phases may be impurity-stabilized.

layer at the surface edges. However, after the crystal had already been irradiated for 90 min, the condenser aperture was again removed and almost immediately a chunk of the crystal broke away, leaving a thinner specimen as imaged in Fig. 6a. The corresponding electron diffraction pattern indicates weak reflections due to a surface phase located on the top (001) surface. At the clean crystal edge, the image reveals contrast due to regions of as-yet undamaged L-Ta_2O_5.

After continued irradiation for 90 min, the surface edge went amorphous as seen in Fig. 6b. After 90 additional minutes of high-flux irradiation, as indicated in Fig. 6c, fringes 2.23 Å apart were visible at the surface edges. Note also that the electron diffraction pattern reveals relatively strong reflections due to the surface phase, evidence of which is visible in the bulk region of the image. These reflections correspond to the [66$\bar{3}$] projection of Ta_2O, as also observed for the [001] specimen discussed earlier. The epitaxial relationship is as follows:

($\bar{1}22$) Ta_2O ‖ ($5\bar{1}0$) L-Ta_2O_5 (U_3O_8-type subcell)

($2\bar{1}2$) Ta_2O ‖ ($\bar{1}\bar{3}0$) L-Ta_2O_5 (U_3O_8-type subcell)

(114) Ta_2O ‖ ($1\bar{1}0$) L-Ta_2O_5 (U_3O_8-type subcell).

The one-dimensional fringes at the surface edges with spacings of 2.23 Å are also due to Ta_2O.

As mentioned, crystals in other orientations damage more readily than [001] specimens; however, they do not necessarily damage any more extensively. Figure 7 shows a time sequence of images from an [020] crystal subjected to a high-flux beam, with the image of Fig. 7a indicating an initially well-ordered structure having a clean surface. The image obtained after 5 min irradiation with the condenser aperture removed is shown in Fig. 7b, and reveals the formation of an amorphous layer at the surface edges with noticeable changes at the (010) surface as well. After 30 min irradiation the formation of a new phase in the amorphous region is apparent, as seen in Fig. 7c. The OD obtained from the region indicated could most closely be indexed as β-Ta oriented along [563], where the β-Ta phase referred to here is reported by Moseley and Seabrook (*17*) as having the β-uranium structure with $a = 10.194$ Å and $c = 5.313$ Å. From an epitaxial point of view this match does not seem likely, so that the phase may actually be an impurity-stabilized phase. TaO_2 (rutile-type) aligned along [020] provided a reasonable match with respect to the spacings; however, the angles disagreed by 4%. The possibility that this is actually an impurity-stabilized phase (whether previously known or unknown) exemplifies a problem often encountered in conventional TEM machines operating at less than UHV pressures. We will elaborate on this point later.

Figure 8a shows an initial image of a Ta_2O_5 specimen in the [200] orientation. Visible in the image are bands of contrast along (200) with a periodicity of approximately $7 \times b$, so that these bands presumably correspond to the folding planes in the $14 \times b$ structure. After 1.5 hr of irradiation with the condensor aperture removed, the surface edge has gone amorphous and a new phase has

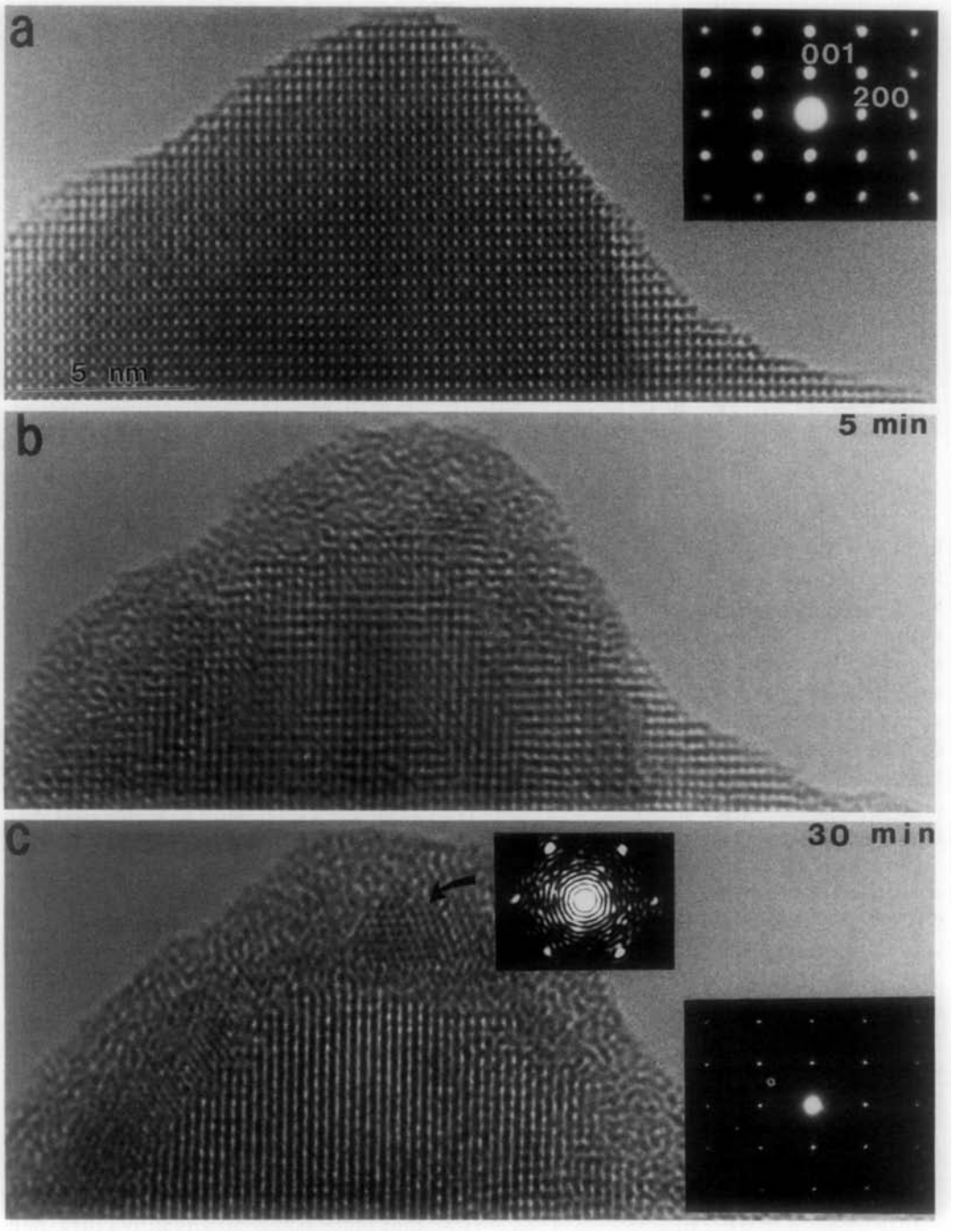

FIG. 7. Time sequence of damage for [020] crystal: (a) Image indicating an initially well-ordered structure. (b) After 5 min irradiation time the structure at the crystal edge appears amorphous. (c) After 30 min irradiation time a new phase has formed in the amorphous region. An optical diffractogram (shown) taken from the region indicated can be indexed as either [563] β-Ta or [020] TaO_2.

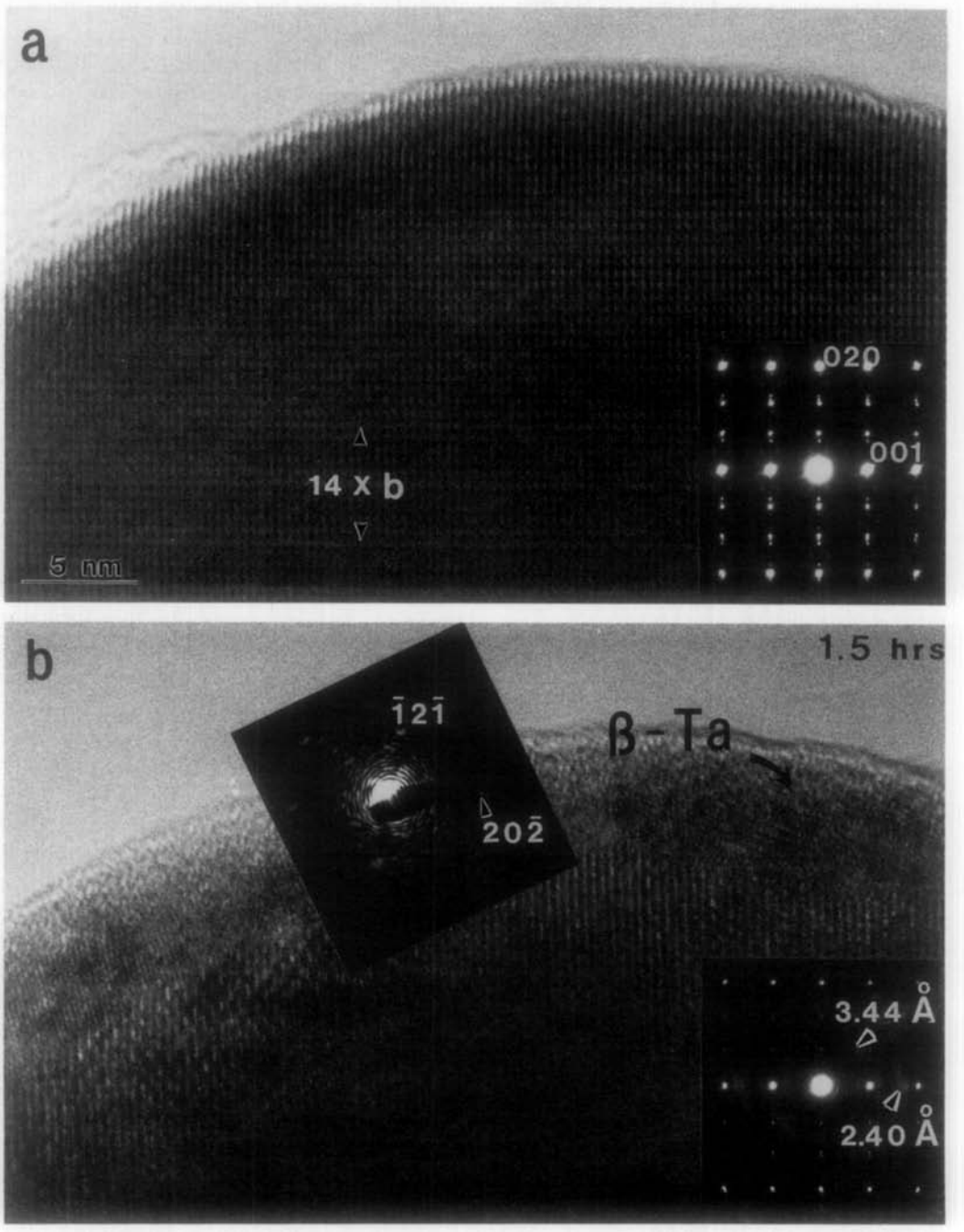

FIG. 8. Image of a specimen aligned along [200]: (a) Initial image. (b) Image taken after 1.5 hr irradiation time. An optical diffractogram taken from the surface region indicated could be indexed as β-Ta aligned along [444]. The spacings of surface reflections on the electron diffraction pattern are labeled.

appeared at the bulk interface as shown in Fig. 8b. Also visible in regions of the top surface are Moiré fringes, and further evidence of a new surface phase is revealed in the corresponding electron diffraction pattern. It should be noted that the reflections along (010) due to the $14 \times b$ lattice are still present, although they are not as predominant as the spots in the pattern of Fig. 8a due to a lesser exposure time. The spacings corresponding to the diffuse reflections due to the surface phase are labeled on the diffraction pattern. These spacings correlate with reflections observed on an optical diffractogram obtained from the surface edge, which could best be indexed as β-Ta aligned along [444]. The optical diffraction data are summarized below:

$(\bar{1}2\bar{1})$ β-Ta (= 3.48 Å) $\|$ (331) Ta_2O_5 (U_3O_8-type subcell)

$(32\bar{1})$ β-Ta (= 2.56 Å $\|$ $(\bar{1}\bar{1}1)$ Ta_2O_5 (U_3O_8-type subcell)

$(20\bar{2})$ β-Ta (= 2.36 Å) $\|$ (001) Ta_2O_5 (U_3O_8-type subcell).

To this point we have seen that L-Ta_2O_5 crystals subjected to high current densities in the H-9000 electron microscope have transformed to the phases Ta_2O and β-Ta or TaO_2. Often transformations of Ta_2O_5 to phases which are probably impurity-stabilized or require impurities to nucleate (*19, 20*) have been observed in this study. For this reason the Ta_2O_5 sample was examined in a UHV HREM, and some results are shown in Fig. 9. The figure shows a time sequence of images of a crystal oriented along [130] irradiated under beam-flux conditions similar to those used in the convention HREM experiments described earlier. Note that the [130] diffraction pattern is almost identical to the [200] pattern seen in Fig. 8, and in fact the relative positions of the Ta atoms for the two orientations are similar in projection. Thus we might expect to observe similar damage products for the two directions, but this does not appear to be the case.

After 60 min exposure to the high-flux beam, one-dimensional fringes due to a new phase (which formed following an amorphous intermediate phase) are clearly visible at the surface edge as seen in Fig. 9b. An OD taken from this region indicates that that lattice spacing is 2.34 Å, and this is also the spacing of strong reflections (arrowed) which appear on the electron diffraction pattern along (001). Note that the other surface phase reflections which appear along (001) are due to double diffraction. Surface reflections (arrowed) along $(3\bar{1}0)$ in the electron diffraction pattern represent a 1.6-Å spacing, which explains why only one-dimensional fringes are visible at the surface edge of the image. These surface reflections index well as [110] bcc Ta, with (002) bcc Ta $\|$ $(3\bar{1}0)$ L-Ta_2O_5, and $(1\bar{1}0)$ bcc Ta $\|$ (001) L-Ta_2O_5. It is not surprising that formation of bcc Ta occurs in a UHV environment, as opposed to formation of impurity-stabilized β-Ta phases.

Discussion

There are of course many events which can occur in an electron microscope to account for specimen damage, ranging from beam-induced chemical reactions to mass loss by knock-on. The details of all mechanisms involved in damaging the specimen cannot be determined unambiguously at present; however, it is possible to deduce the primary mechanism involved from the observations. Regarding the results presented above, we can say that damage is not primarily due to knock-on, since the same experiments reported above were repeated at 100 keV with damage occurring at a faster rate. Preferential loss of oxygen in L-Ta_2O_5 specimens bombarded by electrons has been reported in an Auger study by Lin and Lichtman (*21*); so based on this and the results discussed above (and noting that Ta_2O_5

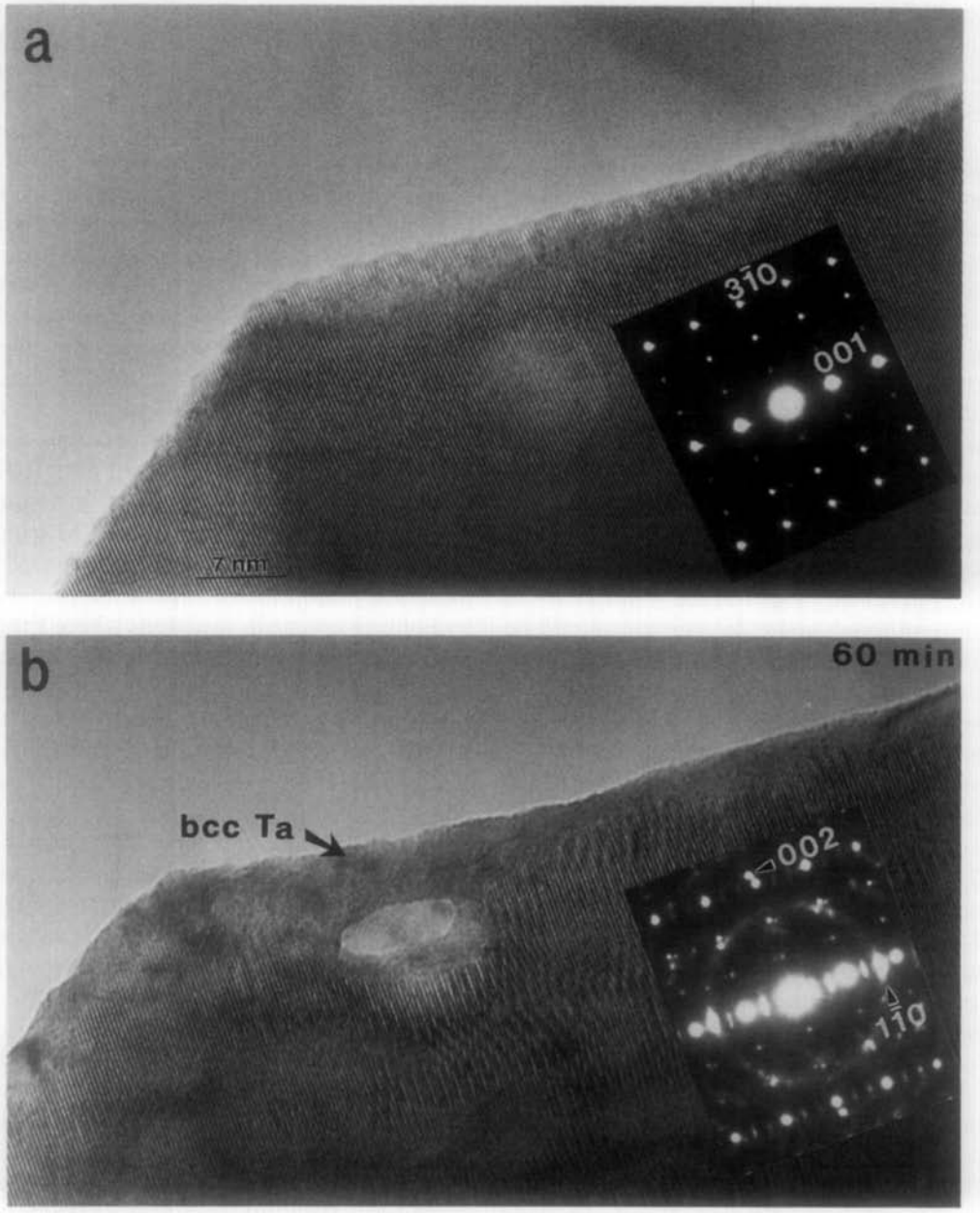

FIG. 9. Images from a [130] specimen taken in a UHV microscope. (a) Initial image. (b) After 60 min irradiation time, bcc Ta aligned along [110] has formed on the (130) surface and at the crystal edge. The arrowed spots on the electron diffraction pattern are indexed with respect to bcc Ta.

is a maximally valent oxide), it is concluded that the primary driving force for phase transformation is desorption of oxygen from the Ta_2O_5 surface (i.e., DIET).

As desorption of oxygen atoms from the specimen surface occurs, the initial structure may become unstable at some point and undergo a phase transition. In the case of L-Ta_2O_5, it is possible that the damage mechanism involves transformation of the 14 × *b* lattice to a lattice having another multiplicity. No such transformation has been observed however, probably because the initial structure of the specimen has a Ta/O ratio near 1 : 2.5—assuming that the crystal chemistry of the 14 × *b* lattice is similar to that described by Stephenson and Roth (*15*) for the 11 × *b* structure. Further loss of oxygen would then result in a Ta/O ratio too high for any superlattice multiplicity to exist, although some oxygen loss could be sustained by preservation of the 14 × *b* lattice after some of the Ta atoms have reduced from Ta^{5+} to Ta^{4+}. Even if this were occurring, however, oxygen loss by DIET would continue until the supply of oxygen atoms at the surface was depleted. This loss of oxygen by DIET would occur far too rapidly for the 14 × *b* lattice to transform to another multiplicity, considering that each of these superlattice structures is very stable. Recall for example that Stephenson and Roth found that the 14 × *b* structure transformed to the 11 × *b* structure only after 2 weeks of annealing at 1350°C.

These arguments are necessarily very simplified; nevertheless new phases do form as a result of beam damage and they are often difficult to identify. Two main reasons for this difficulty are: (i) Many suboxide phases in the Ta–O system do not seem well-characterized, and (ii) some suboxide phases (and metal phases) which have been characterized are impurity stabilized. Thus Dubrovskaya *et al.* (*23*) reported that Ta_2O_5 and Ta were the only pure phases which they could find in the Ta–O system, and Reisman and Holtzberg (*24*) agreed with these results. Table I lists the suboxide and metallic Ta compounds which were used to index the optical diffractograms taken from surface phases. The phases with superscripts were reported either as being impurity-stabilized or as possibly being impurity-stabilized. It remains unclear whether or not the suboxide phases listed are impurity-stabilized.

Many of the suboxide and metallic phases in the Ta–O system have been reported only in isolated studies, suggesting that their compositions and structures depend upon the method of preparation and may indeed be impurity-stabilized. Such was the case for the β-Ta structure discussed above, for example. This in turn suggests that some phases formed in a conventional EM which has a contaminated atmosphere could be previously unobserved. The same possibility holds of course in situations where specimens exposed to air for long periods become contaminated before being introduced into the microscope column. From the UHV HREM experiments, it is interesting to note that a phase reported in the literature as being impurity stabilized has not been observed. For these reasons, it is felt that beam-induced damage experiments conducted in UHV provide the only truly reliable results for determining damage mechanisms. This should be especially true for systems such as Ta–O.

In addition to contamination effects, a symmetry selection rule also appears to be an important factor influencing the phase transformation route, as pointed out by Zhang and Marks (*33*). More specifically, it appears that when damage as initiated primarily by DIET, phase transformation occurs only to new phases having a symmetry higher than that of the initial phase and the two phases have a subgroup–group relationship. In cases such as L-Ta_2O_5 where an amorphous intermediate phase is formed, the final phase is still found to have a symmetry higher than that of the initial structure. According to the symmetry rule, the

explanation for the formation of an intermediate amorphous phase is that a higher symmetry crystalline phase with the correct composition does not exist. In cases where an intermediate crystalline phase does form, it has a symmetry lower than that of the final phase.

Examination of the space groups of the phases shown in Table I reveals that the suboxide and metallic phases observed in this study (viz. TaO_2 rutile-type, Ta_2O, β-Ta, and bcc Ta) tend to have the highest symmetry possible given the composition of the phase. Note that these phases all have a symmetry higher than that of L-Ta_2O_5, which for the purpose of comparison I assume has symmetry *P2mm* or lower. The few phases listed as having a symmetry lower than that of the initial material have never been observed as damage products. The symmetry selection rule could explain why reduction to a monoxide phase was never observed in this study, in spite of the fact that Nb_2O_5, V_2O_5, and TiO_2 are all reported to reduce to the corresponding divalent oxides—it is because the Ta(II)O phases are relatively low-symmetry structures to the phases which are observed.

Acknowledgments

The author acknowledges support from Professor L. D. Marks during completion of this work. This work was supported by the Air Force Office of Scientific Research Grant AFOSR 8609344 DEF.

References

1. M. L. Knotek and P. J. Feibelman, *Phys. Rev. Lett.* **40,** 964 (1978).
2. N. H. Tolk, M. M. Traum, J. C. Tully, and T. E. Madey (Eds.), "Desorption Induced by Electronic Transitions DIET I," Springer-Verlag, New York (1983).
3. W. Brenig and D. Menzel (Eds.), "Desorption Induced by Electronic Transitions DIET II," Springer-Verlag, New York (1985).
4. A. K. Petford, L. D. Marks, and M. O'Keeffe, *Surf. Sci.* **172,** 496 (1986).
5. D. J. Smith and M. R. McCartney, *Ultramicroscopy* **23,** 299 (1987).
6. S. R. Singh and L. D. Marks, *Phil. Mag. Lett.* **60,** 31 (1989).
7. S. R. Singh and L. D. Marks, submitted for publication.
8. J. Strane, M. S. Thesis, Northwestern University (August 1988).
9. H. J. Fan and L. D. Marks, *Ultramicroscopy*, in press.
10. J. Harvey and H. Wilman, *Acta Crystallogr.* **14,** 1278 (1961).
11. L. D. Calvert and P. H. G. Draper, *Canad. J. Chem.* **40,** 1943 (1962).
12. K. Lehovic, *J. Less-Common Met.* **7,** 397 (1964).
13. R. S. Roth and N. C. Stephenson, "The Chemistry of Extended Defects in Non-metallic Solids" (L. Eyring and M. O'Keeffe, Eds.), p. 167, North-Holland, Amsterdam (1970).
14. J. S. Anderson, *J. Chem. Soc. Dalton Trans.* 1107 (1973).
15. N. C. Stephenson and R. S. Roth, *Acta Crystallogr. B* **27,** 1037 (1971).
16. S. Steeb and J. Renner, *J. Less-Common Met.* **9,** 181 (1965).
17. P. T. Moseley and C. J. Seabrook, *Acta Crystallogr. B* **29,** 1170 (1973).
18. G. Das, *Thin Solid Films* **12,** 305 (1972).
19. L. G. Feinstein and R. D. Huttemann, *Thin Solid Films* **16,** 129 (1973).
20. D. W. Face and D. E. Prober, *J. Vac. Sci. Technol. A* **5,** 3408 (1987).
21. T. T. Lin and D. Lichtman, *J. Appl. Phys.* **50,** 1298 (1979).
22. R. Bredeson and P. Kufstad, *Solid State Ionics* **27,** 11 (1988).
23. L. B. Dubrovskaya, G. P. Shveikin, and P. V. Gel'd, *Zh. Neorg. Khim.* **9,** 1182 (1964).
24. A. Reisman and F. Holtzberg, *in* "High Temperature Oxides, Part II," (A. M. Alper, Ed.), p. 217, Academic Press, San Diego (1970).
25. M. H. Read and C. Altman, *Appl. Phys. Lett.* **7,** 51 (1965).
26. R. D. Burbank, *J. Appl. Crystallogr.* **6,** 217 (1973).
27. V. I. Khitrova, V. V. Klechkovskaja, and Z. G. Pinsker, *Soviet Phys. Crystallogr.* **17,** 442 (1972).
28. V. I. Khitrova and V. V. Klechkovskaja, *Kristallografiya,* **27(4),** 736 (1982).
29. V. I. Khitrova, V. V. Klechkovskaja, and Z. G. Pinsker, *Soviet Phys. Crystallogr.* **12,** 907 (1967).
30. Y. Syono, M. Kikuchi, T. Goto, and K. Fukuoka, *J. Solid State Chem.* **50,** 133 (1983).
31. N. Schönberg, *Acta Chem. Scand.* **8,** 240 (1954).
32. N. C. Stephenson and R. S. Roth, *J. Solid State Chem.* **3,** 145 (1971).
33. J. P. Zhang and L. D. Marks, *Surf. Sci.* **222,** 13 (1989).